Available online at www.sciencedirect.com
SCIENCE DIRECT®
International Journal of Heat and Mass Transfer 48 (2005) 1084–1095
International Journal of HEAT and MASS TRANSFER
www.elsevier.com/locate/ijhmt

The effect of the liquid motion induced by air and vapor bubbles on heat transfer around a cylinder

Mohamed A. Atmane [a,*], Darina B. Murray [b]

[a] Civil Engineering Department, University of Alberta, Edmonton, Alta., Canada T6G 2G7
[b] Mechanical Engineering Department, Trinity College Dublin, Dublin 2, Ireland

Received 30 September 2003; received in revised form 16 September 2004
Available online 8 December 2004

Abstract

This paper reports on a study into the effects of bubble-induced motion on heat transfer around a cylinder. Local heat flux due to vapor or air injected bubble motion is measured at different positions around a heated copper cylinder using a hot film technique as well as a heat flux sensor. The first set of experiments, carried out during the first stages of nucleate boiling, showed a dependence of the heat transfer on surface orientation. A similar conclusion was reached in the second set of experiments where the air bubbles were injected using an external source. Average heat flux values computed in the two cases on the upper part of the cylinder were shown to compare relatively well. Finally, the mechanisms involved in the heat transfer enhancement at the same location, on the upper part of the cylinder, in the two sets of experiments are described using a simultaneous analysis of the heat flux time-series and bubble motion.

1. Introduction

Nucleate boiling is well established as a very efficient way to remove heat from solid surfaces. For the same difference in temperature between the bulk liquid and the heated surface, heat transfer rates during nucleate boiling are at least an order of magnitude higher than in natural convection. Two mechanisms contribute to that enhancement: the evaporation process and the agitation created in the liquid phase by the motion of vapor bubbles. The contribution of each of these mechanisms to the total heat flux is not well documented. An attempt is made in this work to experimentally measure, at the surface of a cylinder, the heat flux due to bubble motion with and without evaporation.

The first aim is to evaluate the effect of surface orientation on the heat flux. Dhir [1] has pointed out that the relationship between heat flux and surface orientation is limited to the low heat flux range, i.e. the first stages of nucleate boiling. Nishikawa et al. [2] measured the heat flux at a flat plate with different inclination angles over a large range of wall superheat. They demonstrated that, in the first stages of nucleate boiling, the heat flux was higher for downward facing plates. Cornwell and Grant [3], Yan et al. [4] and Qiu and Dhir [5] focused their experiments on the effect of bubbles sliding along flat or curved surfaces, and showed that the inclination of the surface enhances the heat flux through two separate mechanisms: evaporation through the liquid layer between the bubble and the wall, and the agitation created in the liquid by bubble motion.

* Corresponding author. Tel.: +1 780 492 8088/3188; fax: +1 780 492 0249.
E-mail address: matmane@ualberta.ca (M.A. Atmane).

0017-9310/$ - see front matter © 2004 Elsevier Ltd. All rights reserved.
doi:10.1016/j.ijheatmasstransfer.2004.09.032

Nomenclature

A	area of the hot film
h_{fg}	latent heat of vaporization
hf	heat flux measured from heat flux sensor
k	thermal conductivity of the polyimide substrate
N	number of bubbles released during nucleation
q	heat flux computed from hot film sensor
Q	power dissipated by the hot film
R	resistance
S_H	skewness factor
T	temperature
V	voltage across the compensation bridge during a test
W	volume of vapor bubbles
$\overline{P}$	average of variable P

Greek symbols

β	angular position
δ	thickness of the polymer substrate
ρ_{vapor}	density of vapor
σ_H	standard deviation
ΔT	wall superheat
δT	film overheat

Subscripts

b	bulk water
BM	bubble motion
C	truncated conduction term
CT	total conduction term
film	hot film sensor
M	refers to difference between heat flux prior to and during test
N	nucleation
NC	natural convection
raw	measured directly from hot film sensor
T	total
test	measured during actual test
Top	top arm of the compensation bridge
w	wall (refers to cylinder surface)
0	quantity measured before experiment

Superscripts

copper	cylinder surface
film	hot film sensor

Our second aim is to segregate the heat flux due to evaporation from that resulting from convection in the liquid due to vapor bubbles motion. To do this, we make use of the hot film technique in a system that measures only the heat flux associated with the motion of bubbles. Yoon et al. [6] simulated boiling over a large range of conditions and found that, in nucleate boiling conditions, evaporation accounts for less than 5% of the total heat flux while convection in the liquid contributes up to 80%. Rini et al. [7] obtained a similar result measuring the heat flux during pool boiling of FC-72. The current work based on experiments with and without evaporation will help confirm the trend shown by both studies.

We present finally the results of a comparative study where the heat flux on the upper part of the cylinder is analyzed simultaneously with the bubble motion in both experiments.

2. Experiments and procedures

2.1. Experimental apparatus

The experiments are conducted in an aluminum tank 700 mm high, 600 mm long and 300 mm wide. The tank is equipped with glass windows to allow visual access for the imaging system. The tank is fitted with a copper ceiling on top of which is mounted a pipe. Water from the local supply runs through the pipe in an open loop, maintaining it (and thus the ceiling) at ambient temperature. The external surface of a copper cylinder is used as the test surface. The horizontally mounted cylinder has an outside diameter of 30 mm and is 270 mm long. The cylinder is heated internally using two cartridge heaters (0.5 kW each). The surface of the cylinder has been polished using a fine emery paper. The thickness of the copper wall between the heaters and the cylinder surface is 10 mm. This thickness is sufficient to avoid any heating inertial effects such as those observed by Kenning [8] and which can be responsible for large spatial temperature variations at the cylinder surface.

A high-speed imaging system was used to investigate the vapor bubble dynamics. The system consisted of a high-speed camera (Dalsa CA-D6-0256, 8 bits) capable of taking up to 970 frames per second with a spatial resolution of 260×260 pixels. The camera was equipped in all the experiments with a 75 mm lens. Two frame-grabbers acquired the camera frames in real time and saved them into the memory of a PC. Two different camera positions have been used, depending on what part of the cylinder is under consideration. When focusing on the top and lower parts of the cylinder (respectively

$\beta = 180°$ and $\beta = 0°$), the camera axis was orthogonal to the cylinder axis (both being in the same horizontal plane). For all other angles, the camera axis was at a horizontal angle $\alpha \sim 20°$ from the cylinder axis.

The air bubble injection system consists of a 30 mm by 30 mm matrix on which are fitted nine capillary tubes. All capillary tubes are provided with air by the same cavity housing the matrix. Two sets of tubes, with diameters of 0.3 mm and 1 mm respectively, have been used in the experiments. Air is provided to the cavity through a tank in which the pressure is kept constant at 2 bars. The air flow rate is controlled by varying the opening of a micro-valve mounted between the tank and the air cavity.

2.2. Heat transfer measurement techniques

2.2.1. The hot film technique

A hot film sensor is used to measure the fluctuations in heat flux at the surface of the cylinder. The technique is based on the principle that the energy dissipated by the hot film is proportional to the energy released from the cylinder to the liquid which in turn is proportional to the heat flux at the surface of the cylinder. In order to actively control it, the hot film is maintained at a constant temperature higher than the surrounding cylinder surface by a few degrees δT (defined as the overheat). The technique is similar to that used by Scholten and Murray [9] who successfully measured the surface heat flux from a heated cylinder in a cross-flow of air.

In order to measure the power it dissipates, the film is used in conjunction with a DISA 55M10 compensation bridge. Thus, the film is an arm of a wheatstone bridge connected to a servo-amplifier. The first arm of the bridge is formed of the film and a compensation resistance and the second arm, labeled the top arm, consists of a constant resistance $R_{\mathrm{Top}} = 50.1\ \Omega$. The servo-amplifier measures the imbalance in the bridge and gives as an output the voltage necessary to actively keep the resistance (and therefore temperature) of the film constant. The power dissipated in the film is evaluated from this voltage. The hot film (Senflex model, TAO systems) is made of Nickel and is deposited on an electrically isolating, 50.8 μm thick polyimide substrate (Upilex—thermal conductivity 0.28 W/m K). It is 1.44 mm long, 0.1 mm wide and less than 0.2 μm thick. Two flat copper leads connect the film to insulated electrical wires that carry the fluctuating voltage signal to the compensation bridge. These copper leads are 0.76 mm wide and 12.7 μm thick. The substrate is mounted at the bottom of a depression machined at the surface of the cylinder and curved along its circumference, using a double sided tape rated for high temperature use (MacTac—thermal conductivity 0.18 W/m K) whose thickness is equal to that of the substrate. The hot film is used in association with a T-type thermocouple embedded underneath the film

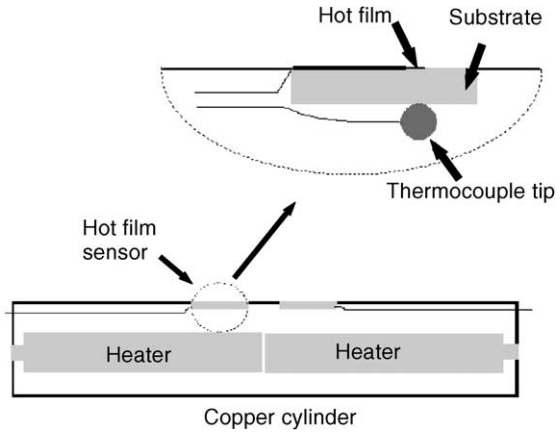

Fig. 1. Schematic view of the test cylinder equipped with the internal heaters. The top drawing shows details of the hot film sensor with the thermocouple underneath it.

(top drawing Fig. 1). The thermocouple tip is 0.7 mm in diameter and has a frequency response of approximately 40 Hz. This thermocouple is used both for surface temperature estimation and for estimation of the hot film heat losses to the substrate. All the wires used to connect the sensor (hot film and thermocouple) to the acquisition system are accommodated in a hole drilled below the surface of the cylinder in order to keep the latter smooth and to avoid surface discontinuities.

2.2.2. The heat flux sensor

A 75 μm thick micro-foil™ heat flux sensor (model 27036-1) manufactured by RdF™ was used to measure the time-averaged surface heat flux. This sensor consists of three layers of a polyimide substrate (Kapton—thermal conductivity 0.16 W/m K) in which are embedded thermopiles at each side of the intermediate layer. The temperature gradient across this layer permits the evaluation of the heat flux through the sensor. The temperature at the top of the middle layer of the sensor can be simultaneously measured by one of the thermocouples mounted at that location. The temperature of the cylinder surface is calculated from the heat flux and the temperature of the embedded thermocouple. The manufacturer specifies a response time of 0.05 s for the heat flux sensor and provides a calibration coefficient that has been verified in natural convection by Atmane et al. [10]. The voltage across the two-thermocouple junction is amplified then digitized via a NI-6024E, 12 bits A/D acquisition board. The absolute uncertainty in the heat flux calculation was evaluated as the standard deviation of the amplified voltage measured when the cylinder was in thermal equilibrium (zero heat flux) in water prior to each run. This was equal to about 220 W/m^2, corresponding to around 1% of the smallest average heat flux measured with this heat flux sensor.

2.3. Hot film sensor calibration and evaluation of heat transfer

In order to calibrate the hot film sensor, the instrumented cylinder was placed inside a thermally insulated box equipped with a heating element, a fan to circulate the air and a pre-calibrated reference thermometer. The air temperature inside the box was increased from 24 °C to 98 °C by steps of 5 °C. At each temperature, the resistance of the film (R_{film}) was measured and the temperature of the embedded thermocouple was read. A plot of the film resistance and the temperature given by the thermocouple against the temperature given by the reference thermometer indicated that both relationships are linear. The calibration range was then extended to 100 °C by carrying out a similar procedure in boiling water. This calibration procedure, that includes a linear least square fitting of the data from the instrumented cylinder versus the reference thermometer, indicated that the uncertainty in temperature is 0.1 °C and that of the film resistance 0.01 Ω.

The film frequency response was evaluated using a square wave test. The test consists of feeding a square wave signal into the bridge and recording the resulting time varying voltage. Analysis of this voltage showed a frequency response of more than 10 kHz when the film overheat is $\delta T = 5.7$ °C. The same overheat was used in all the runs presented in the current work. The total power dissipated in the hot film is calculated as

$$Q_{\text{raw}} = V^2 \frac{R_{\text{film}}}{(R_{\text{film}} + R_{\text{Top}})^2} \tag{1}$$

where R_{film} and R_{Top} are respectively the sensor resistance and the resistance of the top arm of the compensation bridge. V is the voltage necessary to keep the bridge balanced. The corresponding heat flux is calculated by dividing the dissipated power by the area of the film A:

$$q_{\text{raw}} = \frac{Q_{\text{raw}}}{A} \tag{2}$$

The measured heat flux has to be corrected for two contributions that are independent from nucleate boiling. The first contribution originates from the natural convection flow driven by the difference of temperature between the water bulk and the cylinder surface. The average natural convection heat flux around the cylinder was calculated using the correlation of Morgan [11] and modified to reflect changes in the angular position, in accord with the correlation suggested by Kreith and Bohn [12]. The power dissipated in the hot film includes also the contribution of conduction from the film to the cylinder surface, through the isolating substrate. This part is driven by the temperature difference between the hot film and the cylinder surface (therefore, by the film overheat δT). Thus, the second correction q_{CT} to the measured heat flux is the conduction flux from the film to the substrate. The measured flux can then be expressed as

$$q_{\text{BM}} = q_{\text{raw}} - q_{\text{NC}} - q_{\text{CT}} \tag{3}$$

The conduction term q_{CT} can be written as

$$\begin{aligned} q_{\text{CT}} &= \frac{k}{\delta}(T_{\text{test}}^{\text{film}} - T_{\text{test}}^{\text{copper}}) \\ &= \frac{k}{\delta}(T_{\text{test}}^{\text{film}} - T_0^{\text{film}} + T_0^{\text{copper}} - T_{\text{test}}^{\text{copper}} + T_0^{\text{film}} - T_0^{\text{copper}}) \end{aligned} \tag{4}$$

In order to evaluate this conduction term, a preliminary measurement was carried out before each boiling run where the film was overheated and where the cylinder temperature was kept similar to that of the water (close to saturation). The voltage V_0 measured in this manner represents the power dissipated by conduction Q_0 and the corresponding heat flux q_0 is calculated using Eq. (2). In the expression of the total conduction term, we can identify now the flux measured in zero-flow conditions:

$$q_0 = \frac{Q_0}{A} = \frac{k}{\delta}(T_0^{\text{film}} - T_0^{\text{copper}}) \tag{5}$$

The heat flux due to bubble motion can then be rearranged as

$$q_{\text{BM}} = q_{\text{raw}} - q_{\text{NC}} - q_0 - \frac{k}{\delta}(T_{\text{test}}^{\text{film}} - T_0^{\text{film}} + T_0^{\text{copper}} - T_{\text{test}}^{\text{copper}}) \tag{6}$$

or

$$q_{\text{BM}} = q_{\text{M}} - q_{\text{NC}} - q_{\text{C}} \tag{7}$$

where $q_{\text{M}} = q_{\text{raw}} - q_0$ and $q_{\text{C}} = \frac{k}{\delta}(T_{\text{test}}^{\text{film}} - T_0^{\text{film}} + T_0^{\text{copper}} - T_{\text{test}}^{\text{copper}})$.

The calculated flux q_{BM} results only from the passage of the vapor bubbles. That includes the agitation in the liquid created around the bubble as well as the conduction through a liquid layer when the bubble is very close to the heated wall. The nucleation process is not accounted for in the measured flux above because the hot film and its substrate do not contain any nucleation sites. The absence of nucleation on the hot film and its substrate can be explained by the fact that their temperatures (lower than the cylinder surface for the substrate and higher for the hot film) were not high enough to promote nucleation, given the smoothness of their respective surfaces.

Based on the work of Sides [13], the thermocapillary effects have been neglected in the current study. Indeed, that author conducted a theoretical investigation of those effects in subcooled boiling and suggested the use of a non-dimensional number to evaluate their relevance. This factor, based in particular on the residence time of vapor bubbles during nucleation and on the

surface tension, was computed for all the measurement locations in the present study and was found to be smaller than 1, meaning that thermo-capillary motions are not relevant.

2.4. Uncertainty analysis

The uncertainty in the heat flux due to the bubble passage is evaluated from an error propagation analysis for Eq. (7) using procedures described by Moffat [14]. The uncertainty in the first term, the measured heat flux q_M, is evaluated from the systematic error of the output voltages V and V_0, as well as that of the film resistance. The resulting uncertainty in the measured flux is 4%, which corresponds to about 1.45 kW/m^2 for the maximum heat flux. Because it was estimated from a literature correlation (making it impossible to quantify an experimental uncertainty), the natural convection term was assumed to be correct within ±50% of its value. The uncertainty in the last term is evaluated from the systematic error in the temperature measurements estimated during calibration as described in Section 2.3. This uncertainty is about 1.25 kW/m^2. Overall, the combined uncertainty in the heat flux due to bubble motion ranges between 2.8 kW/m^2 at $\beta = 0°$ and 1.8 kW/m^2 at $\beta = 180°$ (respectively 13% and 6% of the local heat flux at that position).

2.5. Experimental procedures

2.5.1. Nucleate boiling experiments

The fluctuations in surface heat flux during boiling at the cylinder surface are evaluated around the circumference of the cylinder at five different locations: $\beta = 0°$, 45°, 90°, 135° and 180°. β is the angle between the vertical and a line joining the cylinder center to the sensor position, with $\beta = 0°$ when the sensor is in the lowest position. Rotation of the cylinder facilitates the measurement of surface heat flux at different surface orientations, from a single hot film sensor. Prior to each experiment, the water temperature is increased using a 3 kW heater mounted in the bottom of the tank. The water is then kept at saturation temperature for at least one hour in order to remove dissolved gases. The heater is then switched off and the internal heaters of the cylinder are turned on in order to initiate the boiling process on the surface of the cylinder. The power of the cylinder heaters is slowly increased until it reaches the maximum. After a steady process is observed, the power is turned down slightly until an excess temperature difference of $\Delta T = 4.5$ °C is reached at the location where the measurement is conducted. Next, the hot film resistance is measured using the compensation bridge and the film temperature is evaluated from the film calibration equation. The hot film temperature is then increased to give a constant overheat in all experiments of $\delta T = 5.7$ °C.

2.5.2. Air bubbles experiments

The cylinder heat flux and temperature were measured at 11 locations. A calibrated T-type thermocouple with a precision of 0.1 °C located close to one of the tank walls, at the same horizontal level as the cylinder, was used to measure the water bulk temperature. A preliminary run where this thermocouple was moved along the water depth has shown that the vertical temperature gradient was not significant. The temperature of the injected air bubbles was not directly measured but calculation of the heat transfer between the water and the air bubbles during bubble rise showed that the bubble temperature is comparable to that of the water at the moment of impact against the cylinder. In all experiments with air bubbles, the water bulk temperature T_b was 11 °C and the cylinder temperature T_w was 17.6 °C.

3. Results and analysis

3.1. Vapor bubble characteristics

The vapor bubble characteristics were calculated at each position for $T_w = 104.5$ °C and $T_b = 98$ °C. The heat flux corresponding to each position is given in the following section. A MATLAB code was written to evaluate the diameter of bubbles as well as their detachment frequencies at $\beta = 0°$ and $\beta = 180°$. For the three other positions, the low contrast in the images made the automatic detection of bubbles ambiguous; the bubble counting and equivalent diameter estimation were then performed manually.

The image processing steps consist of building a Region Of Interest (ROI) containing the bubble and a segmentation operation that separates the bubble volume from the water volume as shown in Fig. 2. A series of erosion and dilation steps are then applied to remove the dark pixels that are not part of the bubble and finally the contour of the bubble is highlighted. The resulting image is then subtracted from a background image taken prior to the experiment containing the cylinder only. The bubble is then labeled and its volume calculated at each time step. The detachment frequency is computed as the number of local maxima in the bubble volume time series over time. The average bubble volume at detachment is taken as the average of all maxima in the bubble volume time series. The results given by this procedure agreed well with the detachment frequency and size evaluated manually for 10 bubbles. This procedure was applied to process two sequences of 2.6 s at each angle. The systematic error in the evaluation of the equivalent diameter is ±2 pixels (approximately ±0.2 mm at $\beta = 90°$ and $\beta = 135°$ and ±0.4 mm at $\beta = 45°$, $\beta = 90°$ and $\beta = 135°$).

The vapor bubble detachment statistics at different locations are shown in Table 1. At the bottom of the

Fig. 2. Views of vapor bubbles before they detach from the lower part of the cylinder (left) and the upper part (right). The spatial scale is the same in both photographs. The dashed lines indicate the Region Of Interest over which the bubbles are detected and the bold lines indicate the detected bubble boundaries.

Table 1
Average bubble release frequency and diameter at detachment from the cylinder during the nucleate boiling experiment at different angles

Angle (deg)	0	45	90	135	180
Release frequency (bubbles per second)	9	30	35	48	25
Average diameter (mm)	7	2.3	2.6	2.4	2.1

cylinder ($\beta = 0°$) the bubble diameter is larger than that measured at the top ($\beta = 180°$). The opposite trend is observed for the detachment frequency. At the three intermediate angular positions, the bubble sizes at detachment are broadly similar and comparable to that measured at the top of the cylinder. The evolution of the detachment frequency is clearer as it increases regularly from $\beta = 0°$ to $\beta = 135°$ and then falls back to a smaller value of 25 Hz at the top of the cylinder. The high detachment frequency observed at $\beta = 135°$ can be explained by an entrainment effect resulting from the passage of bubbles produced at lower positions. Thorncroft et al. [15] have previously observed such an effect on a vertical surface submitted to a flow during the boiling process. In pool boiling experiments of R114 around a cylinder, Barthau [16] found that the diameter at detachment has a maximum at the bottom of the cylinder and then keeps a constant value for intermediate positions before increasing at the top. With the exception of the final point, this trend is similar to that measured in the present study. The detachment frequencies reported by him were also consistent with the trend found in the current work, however, a quantitative comparison is not relevant as his experiments were performed in different experimental conditions (different liquid, different pressure).

3.2. Injected air bubbles

The characteristics of the air bubbles were measured about 3–4 cm below the cylinder. The digital camera was used to record sequences 4 s long at a rate of 500 fps. The images were then processed using a MATLAB code similar to that described above to evaluate the bubble size distributions. The bubble release frequency was measured directly in a different experiment where the camera was directed towards one of the capillary tubes. The sequences were longer (10 s) at a lower frame rate (200 fps).

The average equivalent diameter of the bubble was 12.0 ± 2.7 mm, the release frequency was 40 bubbles per second and the plume width was evaluated as about 30 mm. The void fraction computed based on a square section covering the whole plume was estimated as 13.7%.

3.3. Local variation of the heat flux

Fig. 3 shows the variation as a function of the angular position of the time-averaged heat flux due to vapor bubble motion, q_{BM}, as well as its three components (q_{BM}, q_C and q_{NC}) for the nucleate boiling case. The shape of q_{BM} is similar to that of the measured flux q_M, the changes in the two other components being too small to affect this shape. The heat flux due to bubble motion increases from $\beta = 0°$ to $\beta = 135°$, at which

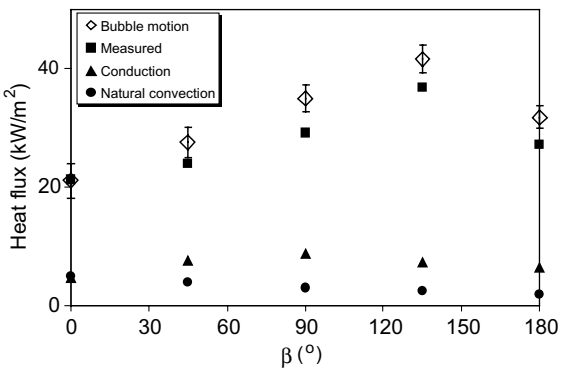

Fig. 3. Profiles of the heat flux during the nucleate boiling process and its components as function of the angular position around the cylinder.

point it reaches a maximum. This maximum is approximately twice the nominal value measured on the lower part of the cylinder. Table 2 contains the standard deviation of the heat flux as well as the relative intensity (defined as the ratio of the standard deviation to the time-averaged measured heat flux). Both quantities show the same trend as the average values.

Fig. 4 shows the local time averaged heat flux profile around the cylinder for the experiment with air injected bubbles. The heat flux is highest on the lower part of the cylinder. It then decreases in the range $\beta = 0°$ to $\beta = 60°$. Beyond that angular position, the heat flux peaks at an angle $\beta = 110°$ then drops again before rising at very high angles.

In order to explain the high heat flux values measured on the lower part of the cylinder, we show in Fig. 5 the time series of the heat flux measured using the heat flux sensor at $\beta = 0°$ when air bubbles are injected below the cylinder. The heat flux is normalized with the nominal value (defined as the base heat flux before the increase) and shows an increase of a factor of more than 4 when a bubble hits the cylinder. The local maxima that follow the first peak are a result of secondary impacts of the bubble. In the same figure is shown the temperature time series during and after the impact. The temperature decreases at the impact then starts to recover towards its initial value. The recovery part is not monotonic because of the secondary impacts.

To evaluate the spatial extent of the effect of the air bubble impact, we show in Fig. 6 the high order statistics

Table 2
Standard deviation and intensity of the fluctuations of heat flux at different locations around the cylinder

Angle (deg)	0	45	90	135	180
Std q_m (kW/m^2)	2.55	4.92	5.70	7.99	4.98
Intensity (%)	10	15.6	15	18	14.8

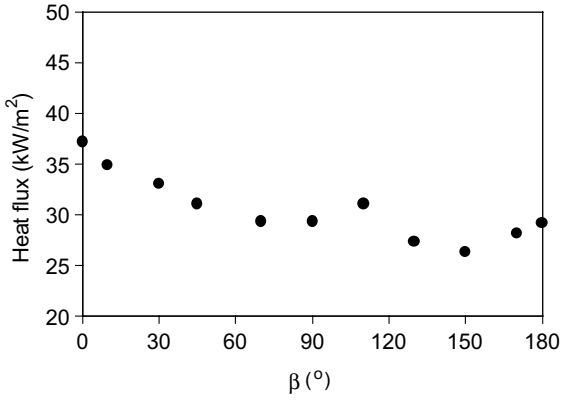

Fig. 4. Profiles of the heat flux when air bubbles are released as function of the angular position around the cylinder.

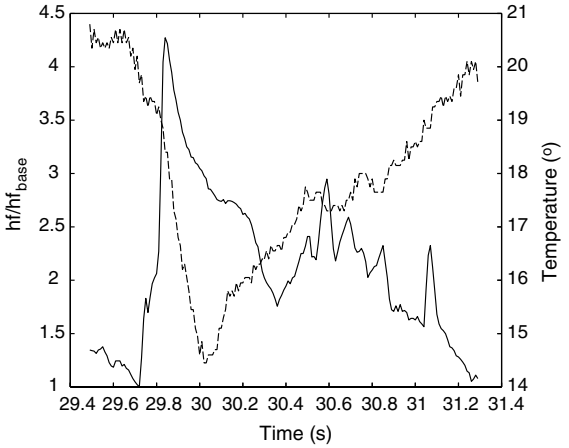

Fig. 5. Time series of the normalized heat flux and temperature recorded at $\beta = 0°$ during the impact of an air bubble. Solid line is normalized heat flux. Dashed line is temperature.

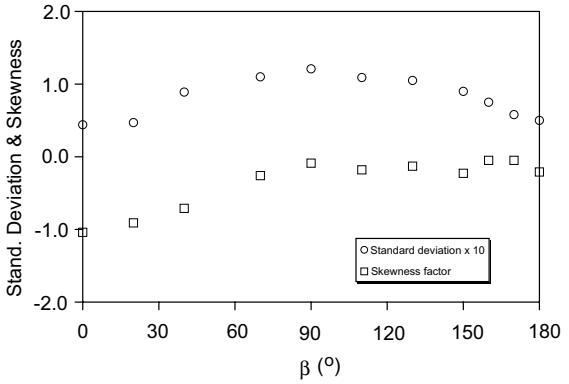

Fig. 6. Variation of the standard deviation and skewness of the heat flux time series as function of the angular position during the release of air bubbles.

of the heat flux time series around the cylinder. Thus, we compute the skewness factor based on the instantaneous heat flux time series (hf(t)), its time averaged heat flux $\overline{\mathrm{hf}}$ and the standard deviation σ_H:

$$S_H = \frac{\overline{(\mathrm{hf}(t) - \overline{\mathrm{hf}})^3}}{\sigma_H^3}$$

The standard deviation σ_H is broadly symmetric around its maximum position located in the intermediate part of the cylinder. Thus, the bubble impact does not seem to contribute significantly to the fluctuations in heat transfer. The skewness factor, which has a value of 3 for a Gaussian distribution, has its maximum absolute value on the lower part of the cylinder. This value is typical of a time series dominated by individual events,

in this case, bubble impacts. Thus, from this profile, we can infer that the limit of the influence of the impact mechanism is located at an angle lower than $\beta = 90°$.

A direct comparison of the profiles with and without boiling over the whole range of angular positions is not possible because of the effect of air bubble impacts on the lower part. However, we note that the average heat flux computed between $\beta = 90°$ to $\beta = 180°$ during boiling is higher only by about 25% than the average flux computed over the same range in the experiments with air bubbles. This indicates that in spite of the differences in the two configurations (in particular, the bubble size distributions), the two heat flux estimates compare relatively well.

3.4. Contribution of bubble motion to heat transfer in nucleate boiling

The relationship between wall superheat and surface heat flux in boiling is strongly dependent on the heating surface. Thus, the Rohsenow correlation [17] for nucleate boiling from a flat surface gives values of 13.1 kW/m^2 and 87.7 kW/m^2 for the present level of wall superheat, depending on whether the copper surface is considered to be 'finely polished' or 'scored' respectively. This range spans the measured heat flux values here but given the difference in geometry and the sensitivity to surface characteristics it is not possible to evaluate the current measurements in this manner.

The average heat flux around the cylinder is $\langle \bar{q}_{BM} \rangle = 31.3$ kW/m^2. This flux is only part of the total heat flux released by the cylinder $\bar{q}_T$, the other part being released through nucleation/evaporation $\bar{q}_N$. In order to compare these two contributions, $\bar{q}_N$ is evaluated using two methods. First, we assume that the energy provided by the internal cylinder heaters ($\bar{q}_T \sim 40$ kW/m^2) is completely dissipated at the surface of the cylinder, and that the heat lost at the two ends of the cylinder can be neglected. An estimate of this heat loss term confirms that it is two orders of magnitude smaller that $\bar{q}_T$. Therefore, the heat flux due to evaporation can be estimated as $\bar{q}_N = \bar{q}_T - \bar{q}_{BM} \sim 8.7$ kW/m^2. Thus, the contribution of the evaporation process is only 22%, the rest being controlled by bubble motion. The second method is based on the calculation of the total volume of vapor produced at the cylinder. If we assume that bubbles detach from the cylinder at all locations with a constant diameter (d), the heat flux resulting from nucleation can be expressed as

$$q_N = h_{fg}\rho_{vapor} f(\beta) W N$$

where h_{fg}, ρ_{vapor}, $f(\beta)$, W and N are respectively the latent heat of vaporization, the water vapor density, the detachment frequency (a function of the angular position), the bubble volume at detachment and the bubble nucleation density on the surface. The bubble nucleation density is defined as the number of bubbles nucleating over a unit area of the cylinder. The upper limit of N can be obtained theoretically by assuming that bubbles of 2 mm (which is broadly representative of the measured bubble size for most measurement locations) in diameter cover the whole cylinder. It is also assumed, in this case, that there are no interactions between these bubbles, such as coalescence. This assumption leads to a value of $N \sim 31.10^4$ m^{-2}. $f(\beta)$ has been evaluated by fitting a third order polynomial to the experimental data. The fact that the vapor bubble size is much larger on the lowest part of the cylinder introduces some errors into our evaluation but the overestimation of the bubble detachment frequency compensates for that. According to this method, the heat flux due to evaporation is $\bar{q}_N \sim 35$ kW/m^2. This value is comparable to the heat flux measured by the sensor in this study, which originated in bubble-induced motion in the liquid phase. This shows that nucleation can at most account for half the total heat released from the cylinder.

In reality, this value of $\bar{q}_N$ represents the upper limit as it is based on the assumption that the cylinder is fully covered by bubbles. From many video sequences recorded at different locations around the circumference of the cylinder during the boiling process, there was no evidence that the cylinder was fully covered with bubbles. Detailed analysis of a number of sequences has shown that in most experiments, the bubble coverage area was an order of magnitude smaller than the total area of the cylinder. Thus, using a more realistic bubble density of $N_1 = N/10$, the phase change contributes a heat flux of $\bar{q}_N \sim 3.5$ kW/m^2. This value is closer to that estimated from the difference between the power dissipated by the heaters and the measured heat flux due to the liquid agitation. Thus, it is considered to be representative of the current test conditions.

The results described here are broadly comparable to those reported by Rini et al. [7]. These authors estimated independently the contributions of bubble nucleation and convection (bubble-induced agitation) to heat transfer in pool boiling of FC-72 at a superheat similar to that of the present study. It was found that nucleation accounted for 35% of the total heat flux, although Rini et al. [7] considered that this value was overestimated. Furthermore, the nucleation site density was much higher than that observed here, which might account for the difference between the percentages reported here and those of Rini et al. [7].

3.5. Local analysis of bubble motion and heat transfer at the cylinder surface

In this section, an attempt is made to clarify the local and instantaneous effect of air and vapor bubble motion on heat transfer at the cylinder surface. The heat flux at the surface of the cylinder is measured simultaneously

with sequences of bubble motion close to the hot film at $\beta = 135°$ during experiments with and without boiling. Images of vapor and air bubbles rising close to the hot film are shown respectively in Fig. 7a and Fig. 8a. In each case, a white line indicates the position of the hot film on the first image. Each sequence is 2.6 s long and contains images taken at 960 fps. The heat flux time series, sampled at a rate of 1 kHz, corresponding to each sequence are shown respectively in Fig. 7b and Fig. 8b.

In order to analyze and compare the two sequences, we define some parameters relating to the bubble characteristics and the heat flux evolution: the bubble equivalent diameter (d), the bubble rising speed (U), a reference time in the heat flux time trace corresponding to the base heat flux (τ_1), the time at which the heat flux is maximum (τ_2), the time at which the heat flux decays to its initial value (τ_3), the time at which the leading edge of the bubble is at the hot film level (τ_4), the time at which the trailing edge of the bubble is at the hot film level (τ_5), the difference between the maximum heat flux and the base (initial) value (A) and the influence distance of the bubble wake ($L = U(\tau_3 - \tau_5)$). The bubble equivalent diameter and the bubble rising speed are estimated from the analyzed images and the times τ_4 and τ_5 are prone to a relatively large error as they have been visually evaluated. These parameters are given in Table 3 for experiments with and without boiling.

The heat flux increase (A) is higher for the vapor bubble and that can be attributed to the larger size of the bubble. In both cases, the maximum heat flux takes place when the bubble has gone beyond the horizontal plane of the sensor ($\tau_4 < \tau_5 < \tau_2$). It means that the heat flux from the cylinder is still affected by the bubble motion even after it has passed by and that the bubble wake is significant in a similar manner in both cases. Quantitatively, the relative distance over which the bubble wake is still significant is evaluated as L/d. It is equal

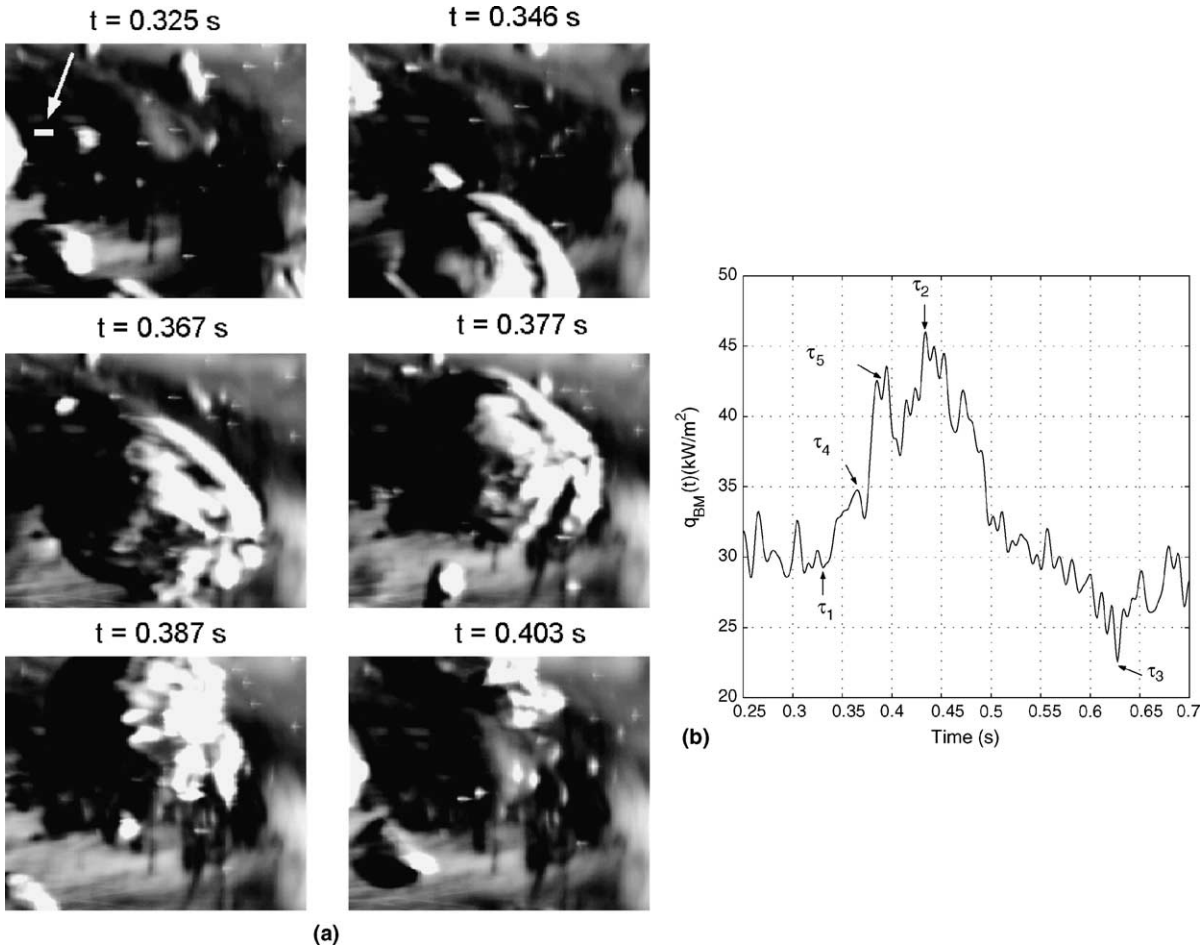

Fig. 7. (a) Sequence of images depicting the vapor bubble motion along the cylinder surface at $\beta = 135°$. (b) Corresponding heat flux recorded by the hot film sensor.

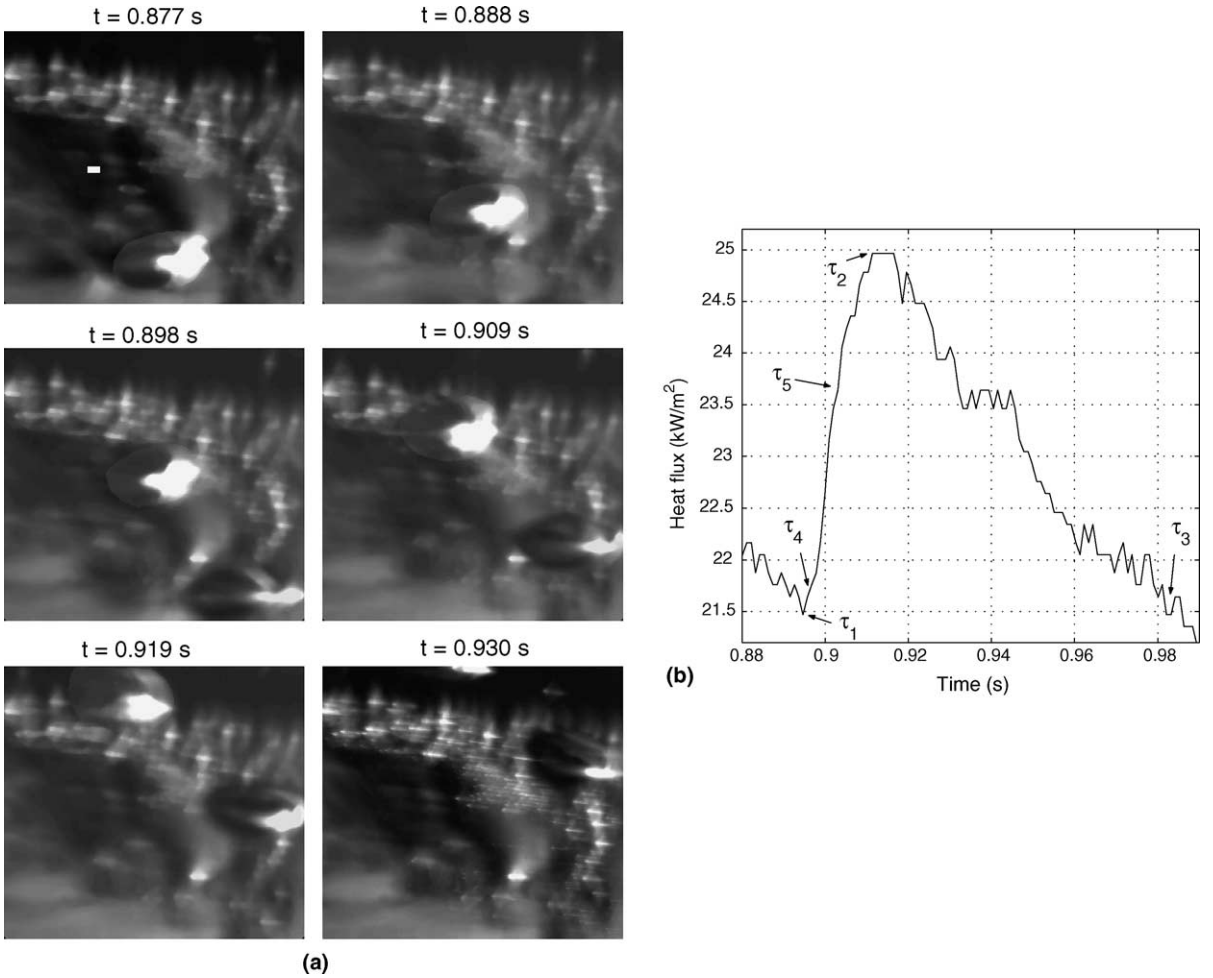

Fig. 8. (a) Sequence of images depicting the air injected bubble motion along the cylinder surface at $\beta = 135°$. (b) Corresponding heat flux recorded by the hot film sensor.

Table 3
Bubble and heat transfer characteristics in the motion-heat flux analysis at two different locations

β	d (mm)	U (cm/s)	τ_1 (s)	τ_2 (s)	τ_3 (s)	τ_4 (s)	τ_5 (s)	A (kW/m^2)	L (mm)
Air bubble	4	28	0.894	0.910	0.982	0.896	0.903	3.5	22
Vapor bubble	14	24	0.325	0.434	0.625	0.367	0.395	15	55.2

to $L/d = 5.5$ and $L/d = 3.9$ respectively for the air and vapor bubbles.

The same analysis has been repeated in both experiments for the passage of several vapor and air bubbles in order to verify the reproducibility of the decay part of the curves obtained above. Thus the decay curves recorded after the passage of 12 vapor bubbles and 8 air bubbles have been isolated. In order to compare them, the decay curves have been normalized so that the heat flux values range between 0 and 1, then averaged. The average decay curves are depicted in Fig. 9. For each experiment, we also show the envelope decay curves representing the curves with the fastest and slowest decay rates. We observe that it takes longer for the heat flux to recover its base value (0) in the case of the air injected bubble (more than 1 s) in comparison with the vapor bubble (about 0.25 s). However, the slope of the curve for air bubbles after 0.5 is almost flat which indicates a possible effect of the way the ensemble average was computed. A better way to compare the two decay curves is

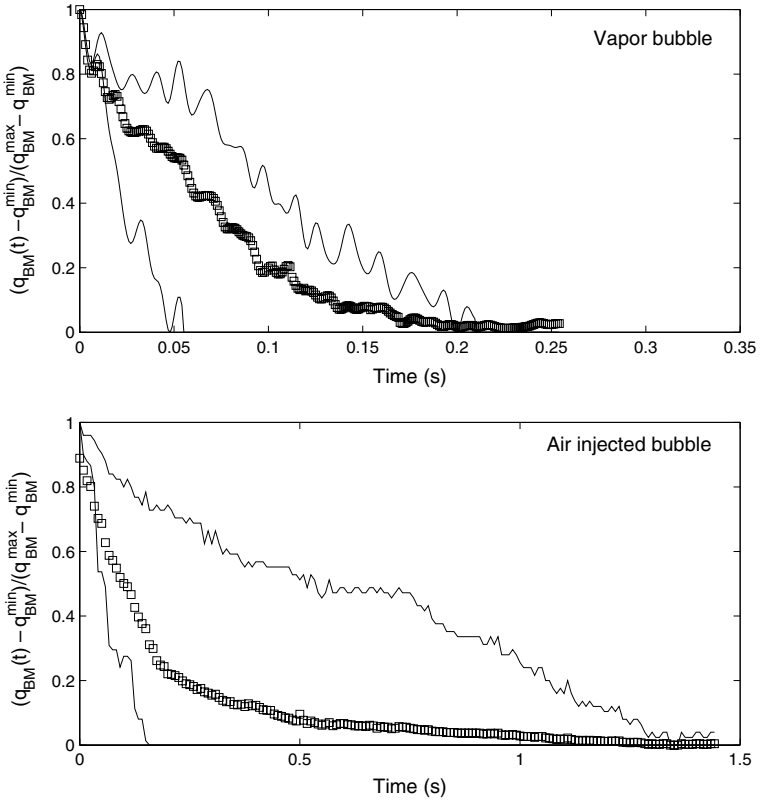

Fig. 9. Normalized heat flux decay curves recorded after the passage of vapor and air injected bubbles at $\beta = 135°$. In each graph, the squares are the ensemble average computed using 12 (vapor) and 8 (injected air) decay curves. The lines are the envelopes of the 12 (respectively 8) curves.

to see how long it takes the heat flux to reach a certain percentage of the maximum value. If we consider a typical value of 20%, we see that it takes on average 0.1 s for vapor bubbles and less than 0.2 s for air bubbles to reach that level, which are comparable values. We also notice that the envelopes spread over a larger range of heat fluxes for air bubbles. That can originate either from the larger distribution of air bubble sizes or a significant difference in the distances between the rising bubbles and the cylinder surface. We note that this distance has not been exactly measured here but it was made sure in all the events included in this analysis that the bubbles passed very close to the cylinder. It was also important to ensure that all the decay curves were caused by a single bubble passing close by the cylinder surface.

4. Conclusion

Heat transfer at the surface of a horizontal, circular cylinder has been investigated under the effect of nucleated vapor and air injected bubbles. A hot film technique and a heat flux sensor have been used to evaluate local time varying convective heat flux at different positions around the cylinder circumference. It was found that during nucleate boiling heat transfer is highest on the upper part of the cylinder, following the detachment of vapor bubbles that have been sliding along the cylinder. The bubble impact mechanism in the case of injected bubbles increased the heat transfer on the lower part of the cylinder. A comparison of the local averaged heat flux on the upper part of the cylinder showed that these values compared relatively well in the two cases (with and without nucleate boiling). Using two different methods to estimate the heat flux due to evaporation, it was found that the nucleation/evaporation process accounts for only a small part of the total heat flux at low wall superheat.

Finally, heat transfer mechanisms have been investigated on the upper part of the cylinder in the two experiments. The heat transfer enhancement is mainly associated with the liquid agitation due to the bubble wake. This variation in dominant heat transfer mechanisms can explain the location of the maximum heat flux recorded at $\beta = 135°$ during boiling.

Acknowledgment

Financial support for this work was provided by the Basic Research program of Enterprise Ireland, under research grant no. SC/1998/711.

References

[1] V.K. Dhir, Boiling heat transfer, Ann. Rev. Fluid Mech. 30 (1998) 365–401.
[2] K. Nishikawa, Y. Fujita, H. Ohta, Effect of surface configuration on nucleate boiling heat transfer, Int. J. Heat Mass Transfer 27 (1974) 1559–1571.
[3] K. Cornwell, I.A. Grant, Heat transfer to bubbles under a horizontal tube, Int. J. Heat Mass Transfer 41 (10) (1998) 1189–1197.
[4] Y. Yan, D. Kenning, K. Cornwell, Sliding and sticking vapor bubbles under inclined plane and curved surfaces, Int. J. Refrig. 40 (15) (1997) 583–591.
[5] D. Qiu, V.J. Dhir, Experimental study of flow pattern and heat transfer associated with a bubble sliding on downward facing inclined surfaces, Exp. Therm. Fluid Sci. 26 (2002) 605–616.
[6] H.Y. Yoon, S. Koshizuka, Y. Oka, Direct calculation of bubble growth, departure and rise in nucleate pool boiling, Int. J. Multiphase Flow 27 (2001) 277–298.
[7] D.P. Rini, R.H. Chen, L.C. Chow, Bubble behavior and heat transfer mechanism in FC-72 pool boiling, Exp. Heat Transfer 14 (2001) 27–44.
[8] D.R. Kenning, Wall temperature patterns in nucleate boiling, Int. J. Heat Mass Transfer 35 (1) (1992) 73–86.
[9] J.W. Scholten, D.B. Murray, Unsteady heat transfer and velocity of a cylinder in cross flow, Int. J. Heat Mass Transfer 41 (10) (1998) 1139–1156.
[10] M.A. Atmane, V.S. Chan, D.B. Murray, Natural convection around a horizontal heated cylinder: the effect of vertical confinement, Int. J. Heat Mass Transfer 46 (2003) 3661–3672.
[11] V.T. Morgan, The overall convective heat transfer from smooth circular cylinders, in: Irvine, Hartnett (Eds.), Advances in Heat Transfer, Academic Press, New York, 1975, pp. 199–264.
[12] F. Kreith, M.S. Bohn, Principles of Heat Transfer, fifth ed., Boston PWS Pub, 1997.
[13] P.J. Sides, A thermocapillary mechanism for lateral motion of bubbles on a heated surface during subcooled nucleate boiling, J. Heat Transfer 124 (2002) 1203–1206.
[14] R.J. Moffat, in: Azar (Ed.), Uncertainty Analysis, in Thermal Measurements in Electronics Coolings, CRC Press, New York, 1997, p. 45.
[15] G.E. Thorncroft, J.F. Klausner, R. Mei, An experimental investigation of bubble growth and detachment in vertical upflow and downflow boiling, Int. J. Heat Mass Transfer 41 (1998) 3857–3871.
[16] G. Barthau, Active nucleation site density and pool boiling heat transfer—an experimental study, Int. J. Heat Mass Transfer 35 (2) (1992) 271–278.
[17] W.M. Rohsenow, in: W.M. Rohsenow (Ed.), Developments in Heat Transfer, The MIT Press, 1964, pp. 169–260.